Orion's Dragon and other stories: Feedback by massive stars

Pabst, C.H.M.

3

Disruption of the Orion molecular core 1 by wind from the massive star θ^1 Orionis C

C. Pabst, R. Higgins, J. R. Goicoechea, D. Teyssier, O. Berné, E. Chambers, M. Wolfire, S. T. Suri, R. Guesten, J. Stutzki, U. U. Graf, C. Risacher, A. G. G. M. Tielens

Nature 565, 618 (2019)

Massive stars inject mechanical and radiative energy into the surrounding environment, which stirs it up, heats the gas, produces cloud and intercloud phases in the interstellar medium, and disrupts molecular clouds (the birth sites of new stars; McKee & Ostriker 1977; Kim et al. 2013). Stellar winds, supernova explosions and ionization by ultraviolet photons control the lifetimes of molecular clouds (Williams & McKee 1997; Wareing et al. 2018; Naiman et al. 2018; Peters et al. 2017; Dale et al. 2014). Theoretical studies predict that momentum injection by radiation should dominate that by stellar winds (Haid et al. 2018), but this has been difficult to assess observationally. Velocity-resolved large-scale images in the fine-structure line of ionized carbon ([C II]) provide an observational diagnostic for the radiative energy input and the dynamics of the interstellar medium around massive stars. Here we report observations of a one-square-degree region (about 7 parsecs in diameter) of Orion molecular core 1 – the region nearest to Earth that exhibits massive-star formation – at a resolution of 16 arcseconds (0.03 parsecs) in the [C II] line at 1.9 terahertz (158 micrometres). The results reveal that the stellar wind originating from the massive star θ^1 Orionis C has swept up the surrounding material to create a 'bubble' roughly four parsecs in diameter with a 2,600-solar-mass shell, which is expanding at 13 kilometres per second. This finding demonstrates that the mechanical energy from the stellar wind is converted very efficiently into kinetic energy of the shell and causes more disruption of the Orion molecular core 1 than do photo-ionization and evaporation or future supernova explosions.

We surveyed a one-square-degree region of the Orion molecular cloud, centred on the Trapezium cluster (θ^1 Orionis) and the Orion molecular core 1 (OMC-1) behind it. The survey was conducted in the 1.9-THz (158-μm) [C II] fine-structure line using the 14-pixel, heterodyne, high-spectral-resolution spectrometer upGREAT (Risacher et al. 2016) on board the Stratospheric Observatory For Infrared Astronomy (SOFIA; Methods). In Fig. 3.1 we compare the [C II] integrated intensity map with the mid-infrared and far-infrared maps that result from ultraviolet- pumped fluorescence by polycyclic aromatic hydrocarbon molecules and thermal dust continuum emission, respectively. Each map clearly shows the interaction of the Trapezium cluster with the dense molecular core (centre), the large, wind-blown bubble associated with the Orion Veil (south) and the bubble created by the B stars illuminating the reflection nebulae NGC 1973, NGC 1975, and NGC 1977 (north). Here, we focus on the prominent Veil bubble associated with the stellar wind from θ^1 Ori C. This shell consists of neutral atomic H gas and is very prominent in the [C II] map; however, there is no detectable counterpart in carbon monoxide, H_2 or other molecular tracers because the shell is too tenuous for these species to persist (for example, $H_2/H < 2 \times 10^{-4}$ and $C/C^+ = 10^{-4}$; Welty et al. 2012; Jenkins & Tripp 2011). Likewise, the complex pattern of absorption and emission features and the presence of multiple (foreground) components preclude recognition of the large-scale structure of the shell in 21-cm H I studies (van der Werf et al. 2013). X-ray observations (Güdel et al. 2008) have shown that this bubble is filled with tenuous (about $1\,cm^{-3}$) hot (2×10^6 K) gas created by the strong stellar wind (mechanical luminosity $L_w = 8 \times 10^{35}\,erg\,s^{-1}$; Howarth & Prinja 1989; Stahl et al. 1996) from the most massive star in the region, θ^1 Ori C (Fig. 3.8).

Although each infrared image (Fig. 3.1) traces the morphology of the Veil, only [C II] probes the kinematics, because it can use the Doppler effect to measure gas velocities. The high spectral resolution of upGREAT allows a detailed investigation of the dynamics of the gas, revealing the kinematic signature of an expanding half-shell as, with increasing velocity, it displaces further away from the centre of the projected shell

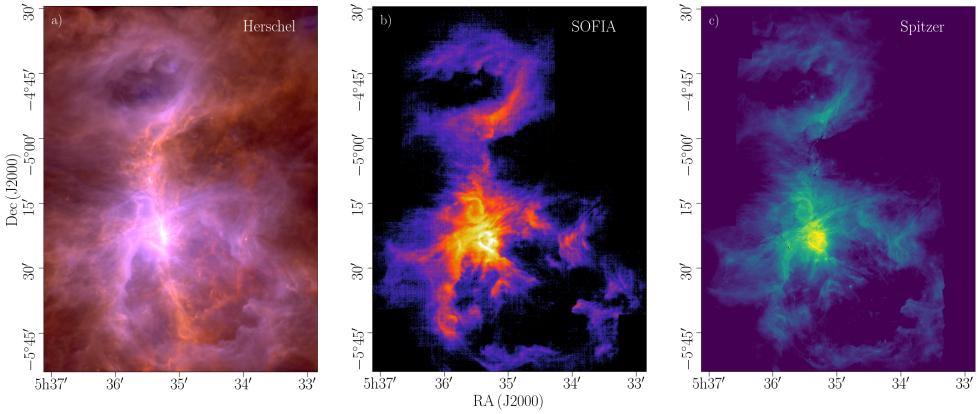

Figure 3.1: Three infrared images of the Orion region of massive star formation. Each of these images shows very similar morphology but in different tracers of the dust and gas in the molecular cloud. a) The dust continuum, observed by the Herschel Space Observatory in far-infrared (blue; using PACS (photodetector array camera and spectrometer)) and sub-millimetre (red; using SPIRE (spectral and photometric imaging receiver)) emission, measures the conversion of far-ultraviolet radiation from massive stars to dust emission in the photodissociation region. b) The integrated 1.9-THz (158-μm) [C II] emission, observed by the upGREAT instrument on board SOFIA, traces the cooling and kinematics of the gas in the photodissociation region. c) The 8-μm polycyclic aromatic hydrocarbon emission, observed by the IRAC instrument on board the Spitzer Space Telescope, outlines the far-ultraviolet-illuminated surfaces of the photodissociation region. A comparison between the three panels does not do justice to the richness of the [C II] data: we can use the roughly 2,200,000 spectra that we obtained to turn this two-dimensional image into a three-dimensional one, enabling a detailed study of the kinematics of the gas.

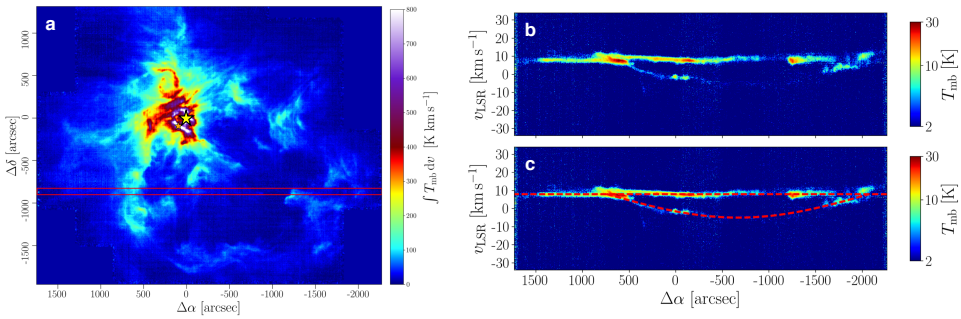

Figure 3.2: Position-velocity diagrams of the [C II] emission along selected cuts across the Veil. a) The Veil bubble in the integrated intensity of the 1.9-THz [C II] emission. The red lines delineate the region over which the spectra were collapsed to produce the east-west cut shown in b and c. The origin (yellow star) corresponds to the position of θ^1 Ori C: right ascension RA(J2000) = 5h 35min 16.46s and declination dec.(J2000) = $-5°\,23'\,22.8''$). The orange star indicates the position of an unrelated star, θ^2 Ori A: RA(J2000) = 5h 35min 22.90s and dec.(J2000) = $-5°\,24'\,57.82''$). b) Position-velocity diagram of the [C II] emission in the east-west cut indicated in a. The velocity shown is measured in the frame of the local standard of rest. Other horizontal and vertical cuts yield similar diagrams (Fig. 3.10). c) A simple model of a spherical half-shell expanding at a constant velocity of 13 km s^{-1} (red dashed lines) is fitted to the data in b. All of the observational position-velocity diagrams are in good agreement with this simple model.

(Fig. 3.9). The kinematic data demonstrate good agreement between the observed velocity structure and a simple model of a half-shell expanding at 13 km s^{-1} towards us while expansion into OMC-1 is stopped by its high density ($n = 10^4$-10^5 cm^{-3}; Fig. 3.2, Fig. 3.10). The small velocity difference (about 1 km s^{-1} towards us) between C^+ and CO emission from the OMC-1 gas represents a slow photo-evaporative flow of atomic gas (H and C^+) into the bubble, where H I is then ionized by extreme-ultraviolet (energy $E > 13.6$ eV) photons from θ^1 Ori C before flowing into the cavity at about 17 km s^{-1} (O'Dell et al. 2017). We determined the mass of gas in the Veil to be between $1,700\,M_\odot$ and $3,400\,M_\odot$, where $M_\odot$ is the mass of the Sun, with a most likely value of $2,600\,M_\odot$ from an analysis of the far-infrared dust emission (Methods). Analysis of the weak [^{13}C II] hyperfine line component that is apparent after averaging over the shell results in a very similar value. This mass estimate is about twice the mass derived from the H I column densities observed along pencil beams towards the Trapezium cluster, which probably reflects known fluctuations in the shell thickness in these directions. The Veil mass that we derive is comparable to the mass of gas in OMC-1 (about $3,000\,M_\odot$; Buckle et al. 2012) and to the mass of the (newly formed) stellar cluster in OMC-1 (about $1,800\,M_\odot$; Hillenbrand 1997), and greatly exceeds the mass of ionized gas ($2\,M_\odot$ in the dense Huygens region and $20\,M_\odot$ in total; Wilson et al. 1997) and the mass of the X-ray-emitting hot plasma ($0.07\,M_\odot$ (Güdel et al. 2008, ; Table 4.8). A schematic of the region is shown in Fig. 3.3.

Adopting a homogeneous cloud and a size of 2 pc, the mass of swept-up material corresponds to an initial H_2 density of 1.4×10^3 cm^{-3}. The radius of the shell is $R_s(t) = [125/(154\pi)]^{1/5}(L_w/\rho_0)^{1/5}t^{3/5}$, where ρ_0 is the initial density and t is time (Weaver et al. 1977), from which we derive an age of 0.2 Myr. This age is in the range of previous (uncertain) estimates of 3×10^4-10^6 yr based on the expansion of the H II region and on the ages of the protoplanetary disks in the Orion nebula and of the stars

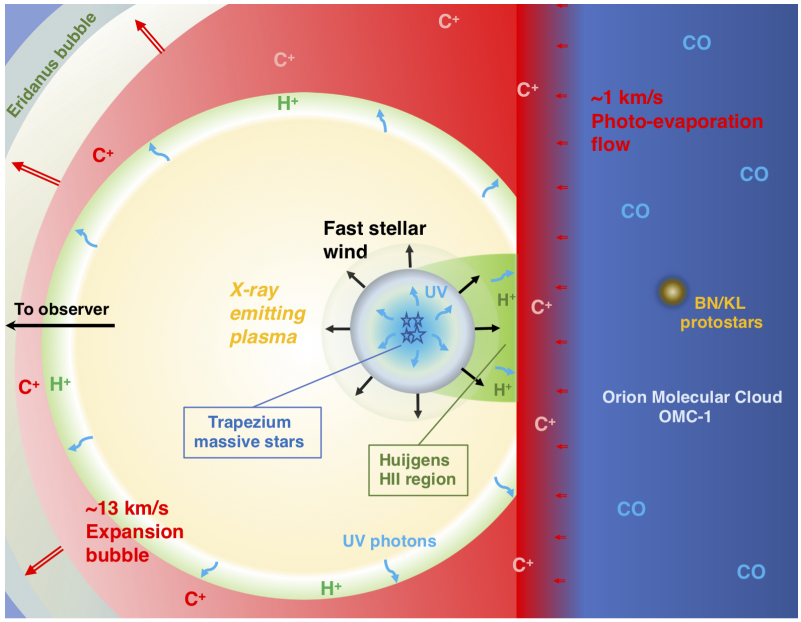

Figure 3.3: Sketch of the structure of the Orion stellar-wind bubble. The stellar wind (black arrows) from the massive star θ^1 Ori C drives a shock into its surroundings which sweeps up the gas. At the same time, this swept-up gas drives another shock (the reverse shock; purple-grey) into the stellar wind, which converts the kinetic motion of the stellar wind into thermal energy, creating a hot (about 2×10^6 K), tenuous (about $1\,\mathrm{cm}^{-3}$), X-ray-emitting plasma (yellow). Adiabatic expansion of this hot gas has swept up the surrounding gas into a slowly expanding ($13\,\mathrm{km\,s}^{-1}$; large red double arrows) 4-pc-diameter half-shell (the Veil bubble; red). The dense Orion molecular core 1 (OMC-1; dark blue) behind the Trapezium cluster (bright blue) stops the bubble expanding in that direction. The BN/KL protostars represent the region of current star formation deep inside OMC-1. Photons with energies of more than 13.6 eV can ionize H to create the dense ionized gas layer (the Huygens region; green) behind the Trapezium cluster, which dominates optical images of the region. This ionized gas expands into the bubble at around $17\,\mathrm{km\,s}^{-1}$ with respect to the background molecular gas. The largely empty interior of the hot gas bubble allows ultraviolet photons (blue wavy arrows) from θ^1 Ori C to travel unimpeded until they interact with the gas and dust in the shell. These photons heat the dust, leading to bright far-infrared continuum emission, and excite large polycyclic aromatic hydrocarbon molecules, producing the 8-μm fluorescence emission (Fig. 3.1a, c). Far-ultraviolet photons will ionize carbon and heat the largely neutral gas in the surface layers of the photodissociation region to about 200 K, causing a gentle ($1\,\mathrm{km\,s}^{-1}$) photo-evaporative flow (small red double arrows). This gas cools through the 1.9-THz [C II] line. On a much larger scale (about 350 pc), the Orion molecular cloud (dark blue) and the Veil bubble (red) are embedded in the Orion-Eridanus superbubble (blue-grey; not to scale).

in the Orion nebula cluster (Hillenbrand 1997; Henney & O'Dell 1999); however, it exceeds the typical dynamical lifetime expected for Trapezium-type multiple systems, 10-50 kyr (Allen et al. 2017). The lifetime of the bubble that we derived (0.2 Myr) and the mass loss rate of θ^1 Ori C imply a total injected stellar mass of $0.08\,M_\odot$, close to the mass of the hot plasma estimated from X-ray observations (Güdel et al. 2008).

We compare the mass, energy and luminosity of the shell to those of other relevant components in Table 4.8. The total kinetic energy of the expanding half-shell is roughly 4×10^{48} erg, comparable to the total mechanical energy delivered by the wind over the age of the bubble (5×10^{48} erg). The total kinetic energy in the ionized gas (6×10^{46} erg) is much less than the kinetic energy of the wind bubble. The X-ray luminosity observed over the age of the bubble is only 3×10^{44} erg and the hot gas expands adiabatically. Assuming that the hot gas fills the cavity, its thermal energy is only around 10^{47} erg (Güdel et al. 2008). Theory predicts that 5/11 of the mechanical energy of the stellar wind will go into heating the hot gas and 6/11 will go into work done on the environment (Weaver et al. 1977). By contrast, we observe that 4/5 of the mechanical energy of the wind has gone into the kinetics of the swept-up shell. This discrepancy may indicate that the bubble is leaking hot gas into the surrounding Orion-Eridanus superbubble (Güdel et al. 2008). However, although detailed inspection of the shell reveals that it is thin in places, the position-velocity diagrams provide no clear kinematic signature of rupture, which would appear as a local, rapid variation in velocity. The radiative luminosity of θ^1 Ori C over 0.2 Myr is 6×10^{51} erg. The kinetic energy of the ionized gas therefore corresponds to an efficiency of 10^{-5} for the coupling of this energy to radial momentum. This efficiency is in good agreement with theoretical studies of this coupling for clouds phases of the interstellar medium (Haid et al. 2018). We note that the radiation pressure ($4 \times 10^4\,\mathrm{cm^{-3}\,K}$) is well below the thermal pressure of the hot gas ($10^6\,\mathrm{cm^{-3}\,K}$) and that the Orion nebula cluster (Orion 1d; see Methods section 'Orion' for a detailed description of the region) is very young (less than 1 Myr), so massive stars have not had time to evolve to the supernova stage. Consequently, neither of these processes will have had a role in the creation of the Veil bubble.

The slow shock that propagates into the environment during the expansion will heat swept-up molecular gas to around 3,000 K; this internal energy is quickly radiated away in high-rotational-level emission of CO and rotational H_2 lines. Such low-velocity shocks do not dissociate or ionize molecular gas, or emit in the [C II] line (Flower & Pineau Des Forêts 2010). The total observed luminosity radiated by dust in the swept-up shell is roughly $6 \times 10^4\,L_\odot$, where $L_\odot$ is the luminosity of the Sun, which results in around 1.5×10^{51} erg over the expansion time of the Veil. The luminosity of θ^1 Ori C provides this energy as stellar photons travel unimpeded through the evacuated cavity, illuminating the inner boundary of the bubble. This excavation turns the [C II] line and the far-infrared and mid-infrared tracers into good tracers of the shell (Fig. 3.1). Observations have shown that gas illuminated by strong radiation fields typically emits between 0.5% and 2% of the stellar photon energy in the 1.9-THz [C II] gas cooling line (Hollenbach & Tielens 1999; Pabst et al. 2017). The stellar far-ultraviolet radiation field is coupled to the gas through the photo-electric effect on polycyclic aromatic hydrocarbon molecules and very small grains (Bakes & Tielens 1994). The [C II] emission (luminosity $L_{\mathrm{C^+}} = 200\,L_\odot$) observed for the Orion Veil translates into a photo-electric efficiency of 0.3%, well in line with these studies. Ultraviolet photon energy that does not go into ionization emerges as the polycyclic aromatic hydrocarbon emission features that so prominently outline the shell (Fig. 3.1).

The velocity of the shell that we derived ($13\,\mathrm{km\,s^{-1}}$) exceeds the escape velocities of OMC-1 (about $2\,\mathrm{km\,s^{-1}}$) and the Orion molecular cloud A (about $8\,\mathrm{km\,s^{-1}}$). Eventually, the wind bubble will break open and vent the hot gas and the ionized gas into the surrounding, tenuous Orion-Eridanus superbubble (Methods). The coasting, neutral shell will then dissolve into the hot plasma. Supernovae typically occur every 1 Myr in the Orion OB 1a and 1b sub-associations (see Methods section 'Orion' for details of the sub-associations) and sweep up all the 'loose' material that has been deposited in the superbubble by bubbles such as the Veil bursting and transport it to the wall of the superbubble (Ochsendorf et al. 2015). In essence, mechanical energy from a supernova (about 10^{51} erg) will go into rejuvenation of the hot gas in the superbubble and transportation of the swept-up gas towards its walls; very little will couple to the Orion molecular clouds A and B. Barnard's loop may be the latest episode in this process (Ochsendorf et al. 2015). Estimates of the proper motion of θ^1 Ori C with respect to the molecular cloud range from about $5\,\mathrm{km\,s^{-1}}$ to $15\,\mathrm{km\,s^{-1}}$, with the latest evidence pointing towards the lower value (Kraus et al. 2009). Therefore, θ^1 Ori C will move about 25 pc away from the cloud before it explodes as a supernova. Hence, like the Orion OB 1a and 1b stars, as a supernova θ^1 Ori C will not affect the evolution of its 'birth' core, OMC-1. Three-dimensional hydrodynamic simulations reveal that, from a theoretical perspective, stellar winds are key to the regulation of star formation through their effect on molecular clouds (Gatto et al. 2017). Here we have analysed one specific case of the interaction of a wind from a massive star with its environment; whether our conclusions apply more generally still needs to be assessed. 1.9-THz [C II] observations with SOFIA are ideal for such studies.

Galaxy formation and evolution result from the combined effects of a complicated set of physical processes that affect the baryons in a ΛCDM (Lambda cold dark matter) cosmology dominated by dark matter. In particular, stellar feedback controls the evolution of galaxies (Naab & Ostriker 2017). Stellar winds from O-type massive stars are very effective at disrupting molecular cores and star formation. Because energy input from stellar wind is dominated by the most massive stars in a cluster whereas that from supernovae is dominated by the more numerous B-type stars, the predominance of the disruption caused by stellar winds has a direct effect on cosmological simulations. As our study shows, relevant stellar feedback processes act on much smaller scales (0.2-2 pc) than are resolved by hydrodynamic studies of the evolution of the interstellar medium (more than 2 pc) or cosmological simulations (more than 50 pc; Kim et al. 2013; Wareing et al. 2018; Naiman et al. 2018; Peters et al. 2017; Dale et al. 2014). 1.9-THz [C II] studies on the dynamic interaction of massive stars through stellar winds with nearby molecular clouds can provide validation for theoretical studies.

Acknowledgements

We acknowledge the work during the upGREAT square degree survey of Orion of the USRA and NASA staff of the Armstrong Flight Research Center in Palmdale and of the Ames Research Center in Mountain View, and the Deutsches SOFIA Institut. Research on the interstellar medium at Leiden Observatory is supported through a Spinoza award. We thank the ERC and the Spanish MCIU for funding support under grants ERC-2013-Syg- 610256-NANOCOSMOS and AYA2017-85111-P, respectively.

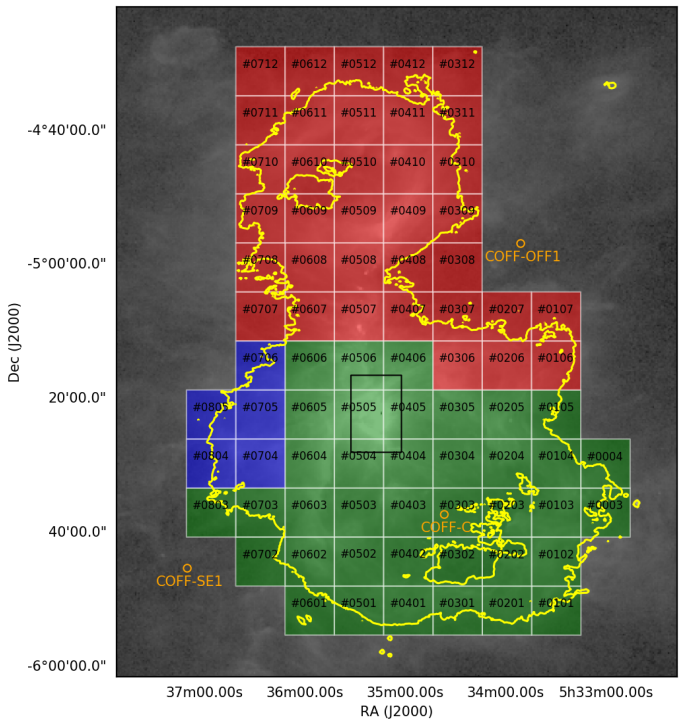

Figure 3.4: Outline of the region mapped in the 1.9-THz [C II] line with upGREAT on SOFIA. The 78 tiles indicated were used to construct the final map. The background image is the 70-μm Herschel/ PACS dust emission. The yellow contours correspond to an approximated far-ultraviolet radiation field of G0 = 50 (in Habing units). The colour of each tile indicates its corresponding OFF position: blue tiles use the COFF-SE1 position, red tiles use COFF-OFF1 and green tiles use COFF-C. Each square tile has a side length of 435.6 arcsec. The black box at the centre indicates the region mapped by the single-pixel Herschel/HIFI instrument in 9h 55min. The total observing time for the SOFIA/upGREAT map was 42 h.

3.A Methods

3.A.1 SOFIA observations

The data presented here were collected using the upGREAT (German Receiver for Astronomy at Terahertz Frequencies) heterodyne receiver on board SOFIA (Welty et al. 2012). SOFIA is an 80/20 joint project between NASA (National Aeronautics and Space Administration) and the DLR (German Aerospace Centre). SOFIA is a modified Boeing 747-SP aircraft with a 2.5-m-diameter telescope mounted in the fuselage aft of the wing (Young et al. 2012). Flying at an altitude of up to 43,000 feet (13 km) provides access to frequencies typically absorbed by the atmosphere. The upGREAT receiver is a heterodyne array receiver with 21 pixels. Two hexagonal arrays each with seven pixels are found in the low-frequency array (LFA), covering a frequency range from 1.81 THz to 2.08 THz. The other seven pixels are found in the high-frequency array (HFA), in a similar hexagonal pattern. The HFA is tuned primarily to the atomic oxygen transition at 4.744 THz. A heterodyne receiver achieves a spectral resolving power of up to $\nu/\Delta\nu = 10^7$ by mixing a locally generated monotone

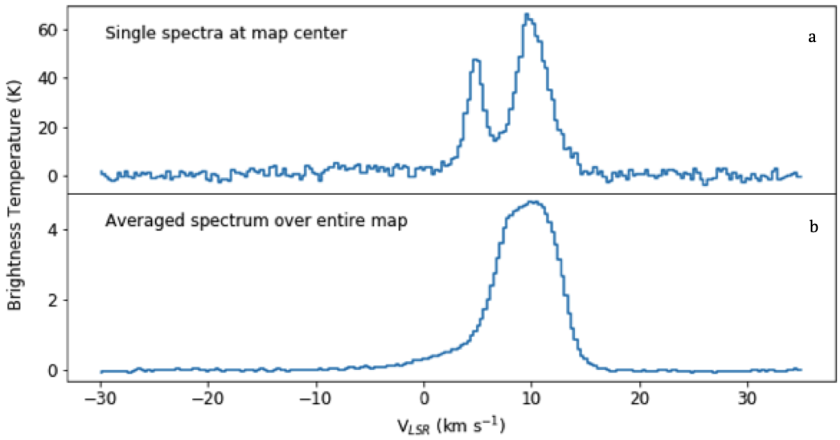

Figure 3.5: Sample 1.9-THz [C II] spectra in our data cube. a) Spectrum obtained at the map centre (RA(J2000) = 5h 35 min 17s; dec.(J2000) = $-5^\circ\,22'\,16.9''$). b) Average spectrum over the entire map.

signal close in frequency to the astronomical signal of interest with the broadband sky signal. The beat tone between the two signals contains the astronomical signal, but at microwave frequencies that can be amplified and sampled using microwave (GHz) electronic components. The original data at a resolution of about $0.04\,\mathrm{km\,s^{-1}}$ was rebinned to $0.2\,\mathrm{km\,s^{-1}}$ to increase the signal-to-noise ratio.

The data was collected using a special array on-the-fly (OTF) mapping mode (Welty et al. 2012). This differs from a classical OTF mode in which a single pixel is traced through the map dimensions and a fully sampled map is generated. In the array OTF observing mode, we use the hexagonal array geometry to generate a fully sampled map. With this approach, each receiver pixel does not cover every map point, but we can map larger regions in the same time as using a classical OTF approach. However, the signal-to-noise ratio is lower and there is some loss of pixel redundancy. The full map region was broken into 78 square tiles of length 435.6 arcsec (Fig. 3.4). Each tile took 22 min to complete. A tile is made up of 84 scan lines separated by 5.2 arcsec. Each tile is covered twice, once in the X and once in the Y direction. Each OTF scan line is made up of 84 dumps of 0.3 s. This returns root-mean-square noise of $T_{\mathrm{mb}} = 1.14$ K per map pixel for a spectral resolution of $0.3\,\mathrm{km\,s^{-1}}$.

The raw data are recorded by a digital spectrometer and come in the form of integer counts per spectrometer channel. These values are converted to antenna temperature using internal hot and cold reference measurements, which establish a scale for the sky measurements. The observation of detected off positions, free from C II emission, is required to remove instrumental artefacts from the data. The next step in the calibration process is to establish the atmospheric transmission and apply it to the astronomical signal. Although SOFIA flies above most of the atmosphere, there are some atmospheric features that need to be considered in the final calibration. The atmospheric emission is determined by fitting an atmospheric model to the off minus internal hot data. The process of atmospheric determination is described in the detail elsewhere (Guan et al. 2012).

Once the atmospheric transmission is applied to each spectrum, a channel map can

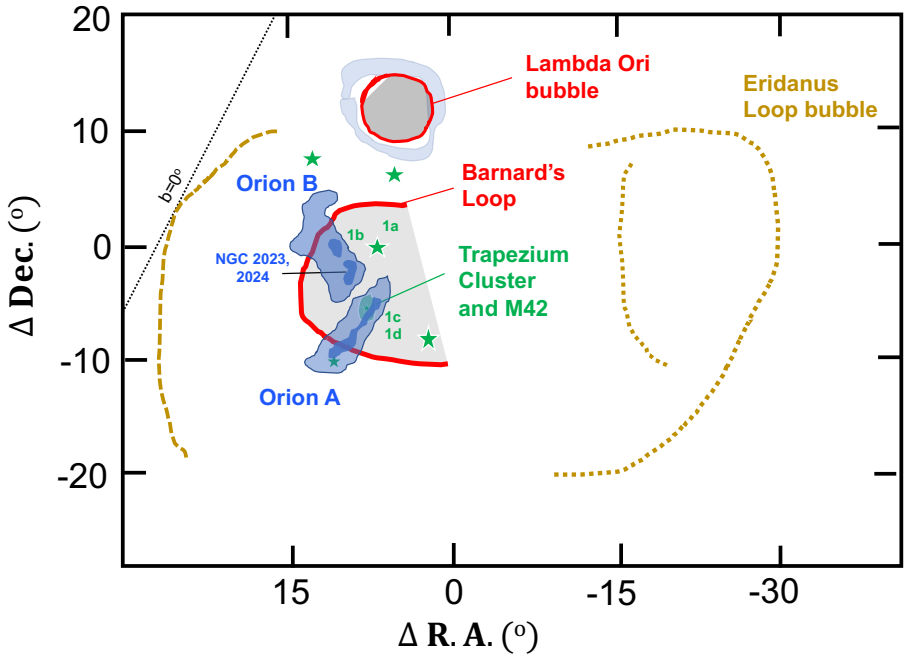

Figure 3.6: Schematic of the large-scale (about 350 pc) structure of Orion. The locations of the massive stars of the Orion constellation are marked with green stars (shoulders and knees; the belt is indicated by a single star; M42 is at the tip of the sword). The two giant molecular clouds A and B are shown in blue, and the prominent H II regions are indicated by the green area, which includes M42 and the Trapezium cluster. Barnard's loop, which is very prominent in Hα, is indicated by the red line. The bubble surrounding λ Ori (grey) is also indicated (red, ionized gas; blue, swept-up molecular shell), as are the boundaries of the superbubble (yellow dashed and dotted lines). Diffuse ionized gas is indicated in grey. The approximate locations of the Orion OB sub-associations – 1a, 1b, 1c and 1d – are marked in green. The dotted line labelled b = 0 indicates the Galactic plane.

be generated. In total 2.2 million spectra were measured. This dataset is converted to a map (Mangum et al. 2007) by defining a map grid; each map pixel is then generated by the distance-weighted sum of all spectra within a given distance of the pixel centre. This begins an iterative process whereby map artefacts are identified and then a correction is applied to the individual spectra and the map is regenerated. The data quality from the upGREAT instrument was exceptional, with 90% of spectra requiring no post-processing. Nominally, problematic spectra could be dropped while still leaving enough for a completely sampled map; however, with the array OTF mapping mode this may not be the case. To recover problematic spectra we developed a spline correction method. The classic approach in heterodyne data processing would be to use a polynomial to remove 'baseline' artefacts from the spectra. However, this can be problematic and is difficult to constrain. We adapted an approach first implemented in the Herschel/HIFI instrument (Kester et al. 2014; Higgins 2011), which used a catalogue of splines generated from data with no astronomical signal. These splines can then be scaled to astronomical data to more effectively remove the baseline. Representative spectra are shown in Fig. 3.5.

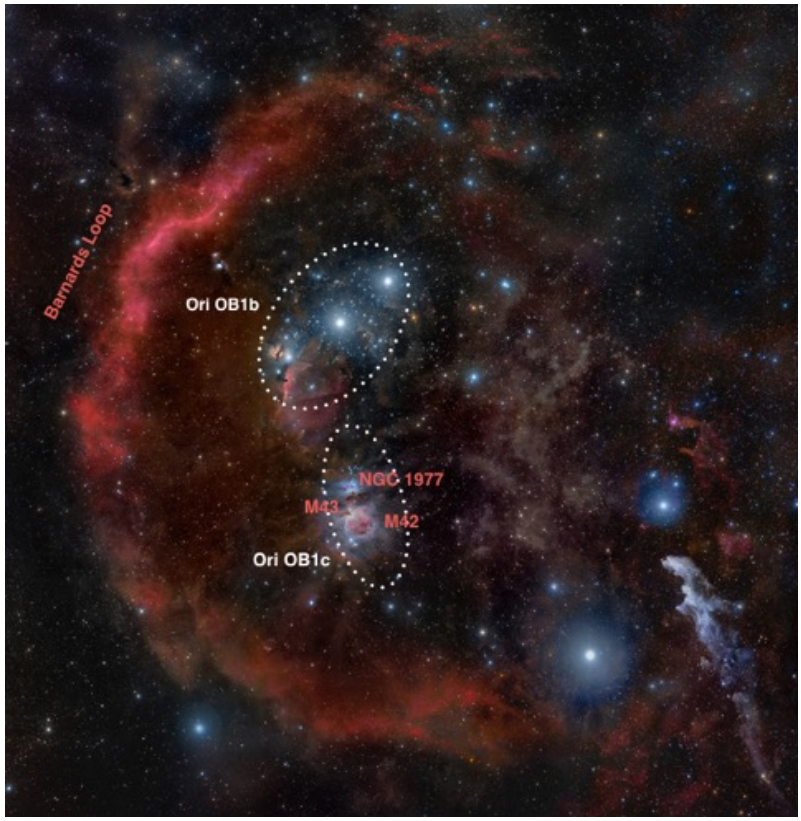

Figure 3.7: Overview of the star-forming region in Orion. The approximate boundaries of the Orion OB associations Ib and Ic are indicated by dashed ellipses. The Orion 1d association is directly associated with the molecular cloud behind the Orion nebula, M42. The reddish glow is due to the Hα line, which originates from recombinations in the ionized gas of Barnard's loop. The belt stars and the knees are obvious. The size of the image is approximately 10^{circ} on the sky.

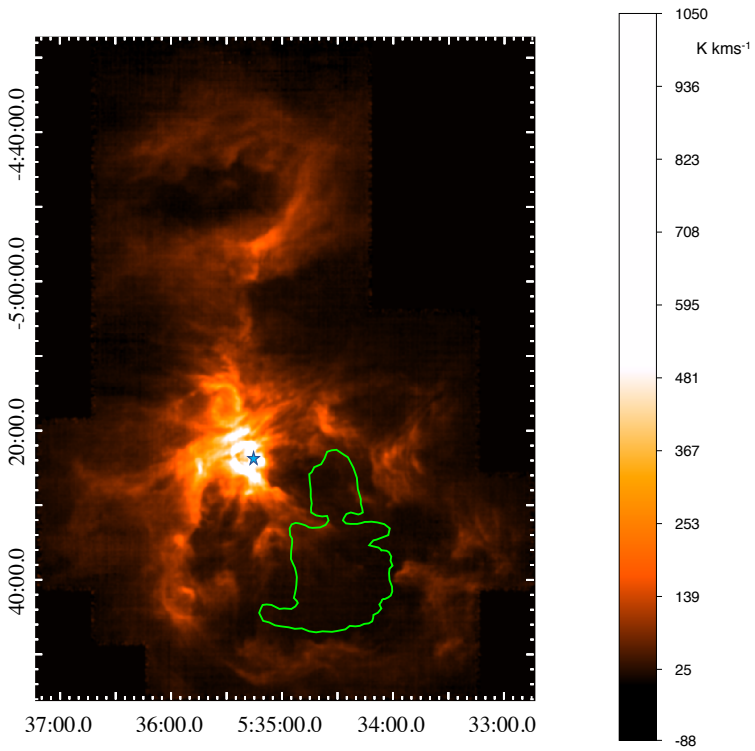

Figure 3.8: Composite infrared and X-ray views of the Orion region of massive star formation. The [C II] integrated intensity map is shown by the colour scale. The X-ray emission (from XMM-Newton) is outlined by a green contour. The hot gas probably entirely fills the bubble, but absorption by the Veil extinguishes the left side. The position of θ^1 Ori C (RA(J2000) = 5h 35min 16.46s, dec.(J2000) = $-5^\circ\,23'\,22.8''$) is indicated by a blue star.

3.A.2 Orion

Orion is the nearest site of massive star formation and has long been used to study the interaction of massive stars with molecular clouds (Elmegreen & Lada 1977; Genzel & Stutzki 1989a). The region contains two molecular clouds, Orion molecular cloud A and B. OMC-1 is one of four cores that have condensed out in the so-called integral-shaped filament that forms the densest part of the Orion molecular cloud A. The distance to the Orion molecular cloud A is known to vary by about 30 pc on a scale of 50 pc (Großschedl et al. 2018), but on the scale of the Orion nebula cluster, the H II region, M42 (the Orion nebula) and the Veil region, the distance is well determined at 414 ± 7 pc (Menten et al. 2007; Zari et al. 2017). This small uncertainty in the distance of OMC-1 does not affect our main results regarding mass or kinetic energy.

The Orion OB associations represent the effects of the ongoing formation of (massive) stars in this region and their interaction with the environment over 10 Myr (Bally 2008). The oldest sub-associations, Orion OB 1a and OB 1b, consist of the stars in the Orion Belt and just north of it (see Figs. 3.6 and 3.7 for an overview of the region). These subgroups have produced several supernovae that have swept up their environment, creating the 350-pc-diameter Orion-Eridanus superbubble. The Orion OB 1c subgroup in the sword is younger (5-8 Myr), and the youngest (less than 1 Myr) stellar subgroup, Orion OB 1d, represents still-active massive star formation associated with the prominent H II regions, M42, M43, and NGC 1977. Part of this subgroup is still embedded in OMC-1.

The Trapezium cluster (θ^1 Ori) is located on the front side of OMC-1. Each of the four stars that make up the Trapezium cluster is a multiple system in itself. θ^1 Ori C is a binary in which the primary has a mass of $34\,M_\odot$ and the companion is only $12\,M_\odot$ (Balega et al. 2015). The spectral type of the primary is O7Vp, with an effective temperature of 39,000 K. θ^1 Ori A and θ^1 Ori D both have much lower mass ($14\,M_\odot$ and $16\,M_\odot$), with spectral type B0.5V. Both are also binary systems with a lower-mass companion (Grellmann et al. 2013). θ^1 Ori B is only $7\,M_\odot$ (Muench et al. 2008). The radiative energy input in the region is dominated by the most massive star, θ^1 Ori C, with the other stars contributing less than 20% of the luminosity of the region. θ^1 Ori C also dominates the ionizing radiation of the cluster (more than 90%). It has a strong stellar wind, with a mass-loss rate of $4 \times 10^{-7}\,M_\odot\,\mathrm{yr}^{-1}$, and a terminal velocity of $2{,}500\,\mathrm{km\,s}^{-1}$, which corresponds to a mechanical luminosity of $L_w = 8 \times 10^{35}\,\mathrm{erg\,s}^{-1}$ (Stahl et al. 1996; O'Dell et al. 2017). Previous estimates (Leitherer 1988) suggest $L_w = 7 \times 10^{35}\,\mathrm{erg\,s}^{-1}$, but this small difference has no influence on our discussion. B0.5 stars have very weak stellar winds and the mechanical energy input by the other Trapezium stars is negligible. The wind from θ^1 Ori C has blown a bubble filled with hot, tenuous gas (density, $n \approx 1\,\mathrm{cm}^{-3}$; temperature, $T \approx 2 \times 10^6$ K; Güdel et al. 2008). This hot gas dominates the diffuse emission at X-ray wavelengths (Fig. 3.8). This bubble is well outlined in the mid-infrared image obtained in the polycyclic aromatic hydrocarbon emission bands and in the far-infrared image of the dust thermal emission (Fig. 3.1). These images trace the interaction of far-ultraviolet (less than 13.6 eV) radiation from θ^1 Ori C with these species in the neutral photodissociation region that separates the hot-bubble gas from the cold material in the molecular cloud.

3.A.3 Kinematics of the gas

Analysis of the individual velocity-channel maps reveals the kinematic signature of an expanding half-shell: with increasing velocity, the shell displaces further away from

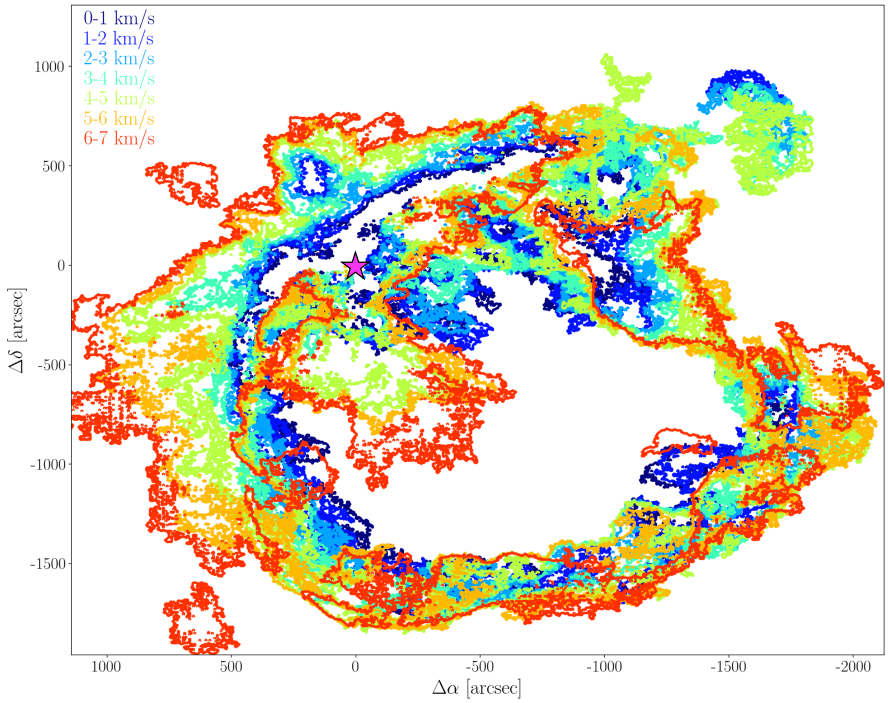

Figure 3.9: Composite figure showing the [C II] emission in different velocity channels. With increasing v_{LSR}, the shell is displaced outwards, away from the centre of the bubble. This is the kinematic signature of an expanding half-shell. Each colour outlines the emission boundaries of channels $1\,\mathrm{km\,s^{-1}}$ wide from $v_{\mathrm{LSR}} = 0\,\mathrm{km\,s^{-1}}$ to $v_{\mathrm{LSR}} = 7\,\mathrm{km\,s^{-1}}$. The origin (magenta star) corresponds to the position of θ^1 Ori C (RA(J2000) = 5h 35min 16.46s, dec.(J2000) = $-5^\circ\,23'\,22.8''$). In the velocity range 4-7 $\mathrm{km\,s^{-1}}$, [C II] emission associated with OMC-4 starts to fill in the interior of the bubble. OMC-4 is a star-forming core near the front of the background molecular cloud and is not part of the Veil bubble.

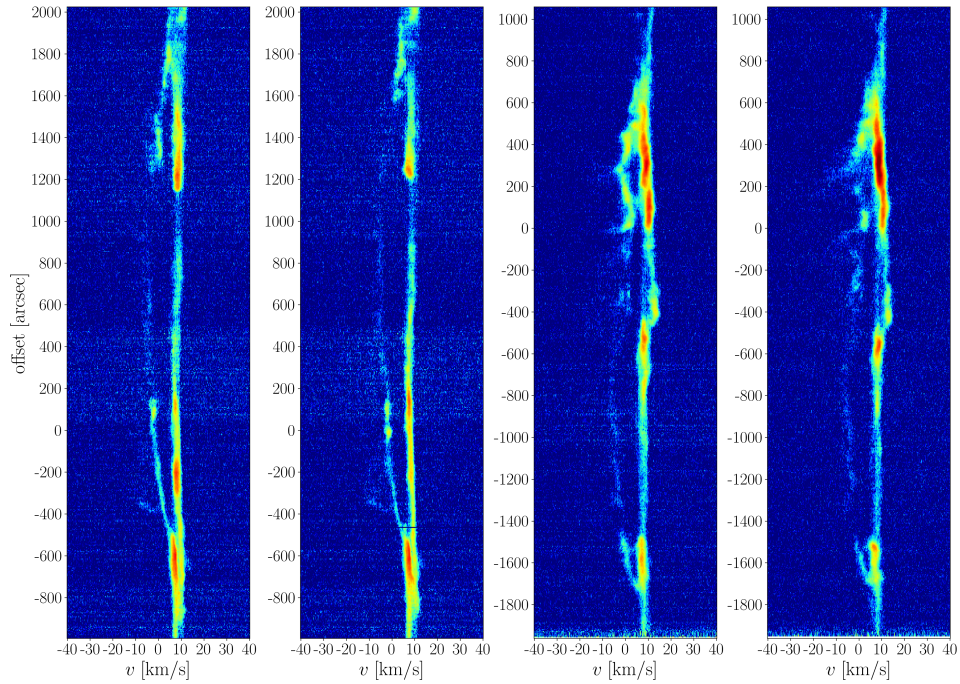

Figure 3.10: Four exemplary position-velocity diagrams of the [C II] emission from selected cuts across the Veil. Each position- velocity diagram exhibits a clear arc structure extending over about $2,500''$, which corresponds to the expanding Veil shell (C.P. et al., manuscript in preparation). The left (right) two panels are cuts along the horizontal (vertical) axis.

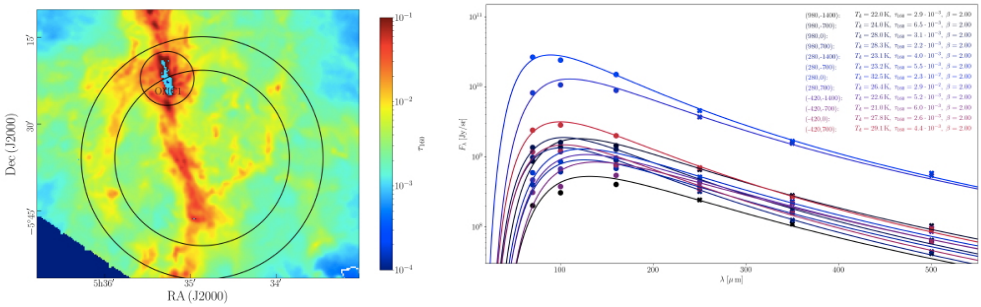

Figure 3.11: Far-infrared dust emission in Orion. Left, optical depth map of the dust emission at 160 μm ($\tau_1 60$), which traces the mass of the shell. The two large circles indicate the extent of the shell used to determine the mass of the limb-brightened shell. The small circle ('OMC1') circumscribes the Huygens region associated with the Trapezium stars. We estimated the mass that is enclosed between the two large circles, excluding the Huygens region. Right, SED of the dust emission observed for different positions in Orion; F_λ is the observed flux. These SEDs are analysed to determine the dust and gas mass. Data and curves represent observed SEDs and model fits for $\beta = 2$, respectively. The legend shows the resulting dust temperature T_d and $\tau_1 60$. These SED fits were analysed for each spatial point and the resulting $\tau_1 60$ values were used to construct the map shown in the left panel.

the centre (Fig. 3.9). We estimate the expansion velocity of the expanding shell of the Orion nebula from position-velocity diagrams. Across the range of the velocity-resolved [C II] map (Fig. 3.2), we build position-velocity diagrams by averaging spectra over cuts that are each 45.5″ wide, along the horizontal and vertical directions (C.P. et al., manuscript in preparation). In Fig. 3.2 we show a representative example of one such diagram; four additional ones are provided in Fig. 3.10. The expanding shell has a clear arc structure that is visible in most of the cuts. From the single position-velocity diagrams that most exhibit this arc, we estimate the expansion velocity by calculating the centroid velocity within the velocity ranges $5\,\mathrm{km\,s^{-1}}$ to $15\,\mathrm{km\,s^{-1}}$ for the [C II] background velocity (at the surface of the molecular cloud) and $-10\,\mathrm{km\,s^{-1}}$ to $5\,\mathrm{km\,s^{-1}}$ for the expanding gas: the difference is the expansion velocity with respect to the background molecular cloud. All [C II] position-velocity diagrams are well described by an expanding-shell model with one central origin and an expansion velocity of $13 \pm 1\,\mathrm{km\,s^{-1}}$ (C.P. et al., manuscript in preparation). Corresponding ^{12}CO(2-1) and ^{13}CO(2-1) position-velocity diagrams46 along the same spatial cut do not show any sign of an expanding shell. This is consistent with the low concentration of molecules in the Veil derived from ultraviolet absorption lines towards the Trapezium stars (Jenkins & Tripp 2011). The position-velocity diagrams reveal that molecular gas is shifted towards slightly higher velocity compared to the [C II] line ($11\,\mathrm{km\,s^{-1}}$ versus $9\,\mathrm{km\,s^{-1}}$).

3.A.4 Mass estimates of the Veil

We estimated the gas mass in the expanding shell from fits to the far-infrared observations of the dust emission using standard dust-to-gas conversion factors (Ochsendorf et al. 2015). We used Herschel far-infrared photometric images in the PACS bands at 70 μm, 100 μm and 160 μm, and the SPIRE bands at 250 μm, 350 μm and 500 μm. We convolved all images to the spatial resolution of the SPIRE 500-μm image (36″). We then fitted the spectral energy distribution (SED) per pixel, using a modified

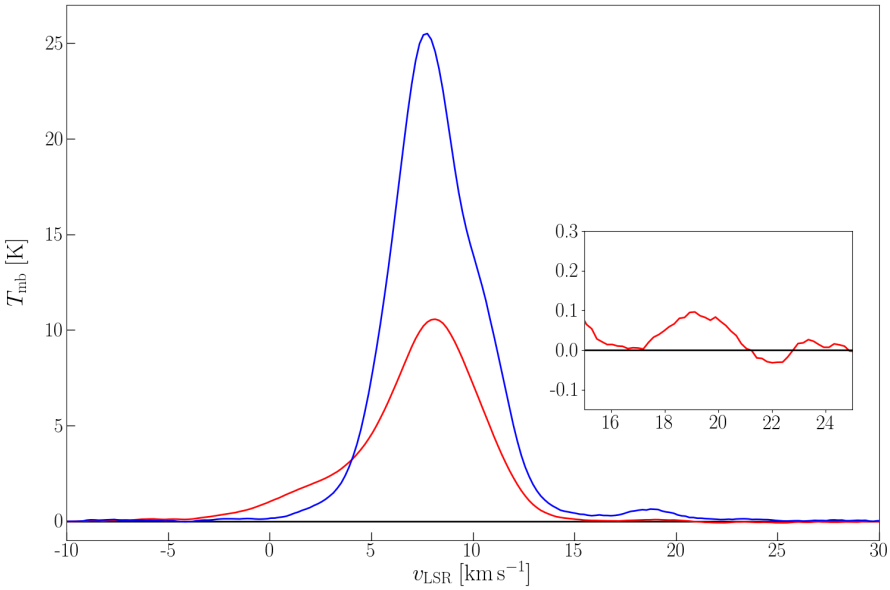

Figure 3.12: Average spectra from the shell. These spectra are dominated by the [C II] line from the main isotope and show the weak hyperfine component of $^{13}C^{+}$ near $v_{\rm LSR} = 20\,{\rm km\,s^{-1}}$. This line is used to estimate the optical depth of the main isotope line and thus the mass of the emitting gas. The red spectrum corresponds to the area between the two large circles in Fig. 3.11, but excluding Huygens region in the small circle. The blue spectrum is an average over the bright parts in the eastern shell, in the declination range $-5^\circ\,35'$ to $-5^\circ\,45'$. The inset shows a close-up of the (faint) [^{13}C II] line in the average shell spectrum.

Table 3.1: Masses, energetics and luminosities in Orion

Component	Mass	Energy		Luminosity	Ref.
		Thermal	Kinetic		
	$M_\odot$	10^{46} erg	10^{46} erg	$L_\odot$	
OMC-1 molecular gas	3000	0.6	20		1
Veil	2600	3	400		8
Stellar cluster	1800	–	–		2
Ionized gas	20	3	6		3, 4
Huygens Region	2	0.3	2		3, 4
Hot gas	0.07	10	–		5
Stellar wind	–	–	500^a	200^b	6, 7
θ^1 Ori C	–	–	–	2.5×10^5	6
FIR dust emission	–	–	–	6×10^4	8
[C II] 1.9 THz	–	–	–	200	8
X-ray	–	–	–	1.4×10^{-2}	5

Notes. $^{(a)}$ Over the calculated lifetime of the bubble. $^{(b)}$ Mechanical luminosity of the wind. References: (1) Buckle et al. (2012), (2) Hillenbrand (1997), (3) O'Dell et al. (2017), (4) Wilson et al. (1997), (5) Güdel et al. (2008), (6) Howarth & Prinja (1989), (7) Stahl et al. (1996), (8) this study.

blackbody distribution:

$$I(\lambda) = B(\lambda, T)[1 - e^{-\tau(\lambda)}],$$

where $\tau(\lambda) = \tau_{160}(160\,\mu\mathrm{m}/\lambda)^{\beta}$, $B(\lambda, T)$ is the Planck black-body spectrum at temperature T and wavelengthλ, and τ_{160} the optical depth at 160 μm. The optical depth of the dust varies with wavelength; this is parameterized by the grain emissivity index β. Typically, β is in the range 1-2. Here, we have chosen $\beta = 2$, in accordance with the standard dust models for $R_V = 5.5$, which are appropriate for the Orion molecular cloud (C.P. et al., manuscript in preparation). Representative fits to the SEDs and the resulting map of the optical depth of the dust are shown in Fig. 3.11. The expanding shell dominates the dust emission in the region in between the two large circles in Fig. 3.11 (see also Fig. 3.1a). The dust emission in the Huygens region, directly surrounding the Trapezium stars, is dominated by the dense photodissociation region that separates the ionized gas from the molecular core. Because this is not part of the expanding shell, we excluded this region (inside the small circle in Fig. 3.11) from our analysis. Using theoretical extinction coefficients (Weingartner & Draine 2001), we obtain a shell mass of $M = 1,700\,M_{\odot}$. There is considerable uncertainty in the SED fit, associated with the exact choice of β. Choosing $\beta = 1.5$, as suggested by the Planck survey (Lombardi et al. 2014), decreases τ_{160} by about 50%, resulting in a derived mass of $900\,M_{\odot}$ using the same theoretical conversion factor as before. Fig. 3.11 shows SED fits towards single points scattered throughout the Orion nebula. Because these are well fitted using $\beta = 2$, the mass estimate of $1,700\,M_{\odot}$ is appropriate. Finally, we have to make a geometric correction because we included the mass only in the limb-brightened shell. Taking the thickness of the shell as 40% of the radius, we obtain a shell mass of $2,600\,M_{\odot}$. Decreasing the thickness of the shell to 20%, the inferred mass increases to $3,400\,M_{\odot}$. Although there is [C II] emission (almost) everywhere, the Veil shows variations in thickness (see below) and the 'front' surface seems to be thinner than the limb-brightened edge.

The shell mass can also be estimated from the [^{13}C II] lines, which are shifted from the [^{12}C II] line owing to hyperfine splitting. Comparison of the strength of the [^{13}C II] hyperfine lines with the (main-component) [^{12}C II] line provides the [C II] optical depth and the excitation temperature with an adopted ^{12}C/^{13}C abundance ratio. These then yield the C^+ column density and, assuming a C abundance, the H column density and gas mass in the region can be derived. However, the [^{13}C II] line is too weak to be detected in the individual spectra. Only by averaging over a large area are we able to detect the strongest of the three [^{13}C II] components, $F = 2 - 1$ [^{13}C II], with a relative strength of 0.625 of the total [^{13}C II] intensity (Ossenkopf et al. 2013). This line is offset by $11.2\,\mathrm{km\,s^{-1}}$ from the [^{12}C II] line (Ossenkopf et al. 2013). The other two [^{13}C II] components, $F = 1 - 1$ and $F = 1 - 0$, lie at $63.2\,\mathrm{km\,s^{-1}}$ and $-65.2\,\mathrm{km\,s^{-1}}$, respectively, and are too weak to be detected in our data. Fig. 3.12 shows the spectrum averaged over the shell (the area indicated by the two large circles in Fig. 3.11). Again, we have excluded the emission from the dense photodissociation region directly behind the Trapezium (the small circle in Fig. 3.11). We also show the spectrum averaged over the brighter southeastern portion of the shell. These two averages both reveal the presence of the [^{13}C II] hyperfine component. The integrated intensity of the [^{i}C II] line is (Tielens & Hollenbach 1985)

$$I_i = B(T_{\mathrm{ex}})\frac{\delta\nu_{\mathrm{D}}}{c}\nu f(\tau_i),$$

where i indicates the isotope, $T_{\rm ex}$ is the excitation temperature, $\delta\nu_{\rm D}$ is the Doppler velocity width, c is the speed of light and ν is the frequency of the line. The factor $f(\tau_i)$ takes optical depth effects into account:

$$f(\tau_i) = 0.428[E_1(2.34\tau_i) + \ln(2.34\tau_i) + 0.57721],$$

where E_1 is the exponential integral. The [^{13}C II] line is optically thin and so $f(\tau_{13})$ is well approximated by $0.625\tau_{13}$, where the numerical factor takes the hyperfine strength into account. The [^{12}C II] line is optically thick and the logarithmic term will dominate. We relate the optical depth of the two isotopes through the carbon isotopic abundance measured for Orion (^{12}C/^{13}C = 67; Penzias et al. 1972), leaving two equations and two unknowns. We analyse the observed intensity ratio of the two lines averaged over the bright portion of the shell – the best determined portion. This results in $\tau_{12} = 3.5 \pm 1.0$ and an excitation temperature of 44 K. With the observed line width ($5\,{\rm km\,s^{-1}}$), we obtain a $^{12}C^+$ column density of $3.5 \times 10^{18}\,{\rm cm^{-2}}$. Assuming that all the gas-phase C is ionized – appropriate for a photodissociation region – and a gas phase carbon abundance (Sofia et al. 2004) of 1.6×10^{-4}, extrapolating these values to the full limb-brightened shell yields an inferred hydrogen mass of $1,700 \pm 400\,M_\odot$. Given the large uncertainties involved, this is gratifyingly similar to the estimate from the dust emission. Correcting for geometry, adopting a shell thickness of 40% of the radius, results in a total mass of $2,600\,M_\odot$. This is an upper limit on the total mass because the brightest portion of the [C II] shell might be characterized by a larger-than-average column density. Also, although the derived optical depth is not sensitive to beam dilution, the derived excitation temperature is. If we were to adopt an excitation temperature of 100 K, the inferred mass, corrected for geometric effects, would be only $1,700\,M_\odot$. The mass of the shell can also be estimated from the observed optical extinction towards the ionized gas in the M42 H II region, because this extinction is dominated by the gas in the Veil (O'Dell et al. 1992). From a comparison of the MUSE Hβ map with the radio emission, an average visual extinction of 1.8 mag is derived (O'Dell & Yusef-Zadeh 2000). Using the theoretical extinction law (Weingartner & Draine 2001) for $R_V = 5.5$, this corresponds to an average H column density of $2 \times 10^{21}\,{\rm cm^{-2}}$. This is half the H column density measured directly towards θ^1 Ori C ($N_{\rm H} = 4.8 \times 10^{21}\,{\rm cm^{-2}}$)11. Adopting this latter value, we arrive at a total mass for the shell ($2\pi R^2 N_{\rm H} \mu m_{\rm H}$, with $m_{\rm H}$ the mass of hydrogen, μ the mean molecular weight and R the radius of the shell) of $1,300\,M_\odot$. The observed extinction is very patchy and the optical nebula seems to be located behind a relative thin portion of the Veil (O'Dell et al. 1992). Hence, we consider this a lower limit. As we consider the dust estimate the most direct measurement of the shell mass, we adopt $2,600\,M_\odot$ for the mass of the Veil in our analysis, recognizing that this value is uncertain by a factor of two.